Numerical modeling of Intensity and phase noise in semiconductor lasers

メタデータ	言語: eng
	出版者:
	公開日: 2017-10-03
	キーワード (Ja):
	キーワード (En):
	作成者:
	メールアドレス:
	所属:
URL	http://hdl.handle.net/2297/1810

Numerical Modeling of Intensity and Phase Noise in Semiconductor Lasers

Moustafa Ahmed, *Member, IEEE*, Minoru Yamada, *Member, IEEE*, and Masayuki Saito

Abstract—A self-consistent numerical approach is demonstrated to analyze intensity and phase noise in semiconductor lasers. The approach takes into account the intrinsic fluctuations of the photon number, carrier number, and phase. A new systematic technique is proposed to generate the Langevin noise sources that derive the laser rate equations keeping their cross-correlations satisfied. The simulation is applied to AlGaAs lasers operating in a single mode. The time-varying profiles of the fluctuating photon and carrier numbers and the instantaneous shift of the oscillating frequency are presented. Statistical analysis of the intensity and phase fluctuations is given. The frequency spectra of intensity and phase noise are calculated with help of the fast Fourier transform. The importance of taking into account the carrier number noise source and its cross-correlation with the noise source on the phase is examined by comparing our results with those by conventional methods.

Index Terms—Fourier transform, noise, numerical modeling, semiconductor lasers, spontaneous emission, time-domain analysis.

I. INTRODUCTION

INTENSITY and phase noise on the output of laser diodes limit their reliability when applied as light sources in optical communication systems, optical discs, optical measuring, etc. The quantum noise corresponds to intrinsic fluctuations in the photon number, carrier number, and phase that are generated during the quantum interaction processes of the lasing field with the injected charge carriers [1], [2]. Excess noise is generated when other effects, such as the re-injection of light by optical feedback, amplify the intrinsic fluctuations. Analysis of the laser noise-types is necessary for further improvement of device performance. Theoretically, this is achieved by mathematical solution of the laser rate equations including Langevin noise sources that account for generation of the fluctuations. Linearization of the rate equations following the small-signal approximation brings about the analytical treatment of the problem [3], [4], which was applied in most of the previous calculations of noise [5]–[12]. However, information concerning the instantaneous fluctuations of the intensity and the phase is missed and, moreover, the accuracy of such an analysis is not guaranteed under large fluctuations.

Direct numerical integration of the rate equations has been applied to overcome the limitations of the small-signal analysis [13]–[23]. Looking into the dynamic behavior of the photon and carrier numbers as well as the phase is a merit of applying the numerical analysis [13]. The Langevin noise sources affecting the photon number, carrier number, and the phase have mutual cross-correlations among them. However, most previous calculations generally ignored the noise source associated with the carrier number [16], [17], [20], [23], or assumed artificial cross-correlations without reporting a solid basis for that assumption [14], [15], [18], [19], [21], [22]. An exception is the calculations of D. Marcuse, who reported a model of intensity fluctuations in which the Langevin noise sources on the photon and carrier numbers are generated with defined auto- and cross-correlations [24]. However, neither the generation of the phase noise source and its cross-correlations to the other sources nor applications to calculate noise were treated.

In this paper, we report a self-contained numerical model to analyze the intensity and phase noise and broadening of the line shape. We demonstrate a new systematic technique to generate the Langevin noise sources on the photon number, carrier number, and phase while keeping their auto- and mutual cross-correlations satisfied. The main idea of the technique is to represent each of the noise sources in a 3-D space of noncorrelated sources in analogy to the conventional vector-representation. Our technique could be understood as a generalization of the method by Marcuse [24]. The time variations of the fluctuating photon number, carrier number and phase are analyzed and their statistics as well. Frequency spectra of both intensity and phase noise are calculated with the help of the fast Fourier transform (FFT). The noise results are compared with those predicted by the small-signal analysis. Moreover, we pay attention to examining the importance of including the noise source on the carrier number in the rate equations, as well as its cross-correlation with the noise source on the phase. We do this examination by comparing our data with those resulting from the approximate calculation of ignoring such random processes.

In the next section, the proposed theoretical model of the numerical simulation is presented, which includes formulation of the laser rate equations and devising a technique to generate the correlated Langevin noise sources. In Section III, the numerical simulation is given for AlGaAs lasers, and the simulated data are compared with those resulting from other methods. Finally, we conclude our work in Section IV.

II. THEORETICAL MODEL

A. Laser Rate Equations

The electric component of the lasing field oscillating at frequency ν is expressed by

$$E(r, t) = \tilde{E}(t)\phi(r)e^{j2\pi\nu t} + \text{c.c.} \qquad (1)$$

where $\tilde{E}(t)$ is a slowly time-varying amplitude of the field, and $\phi(r)$ is its spatial distribution function. Both intensity and phase fluctuations are described by the time variation of the field amplitude [10]

$$\frac{d\tilde{E}}{dt} = \frac{1}{2}(A - G_{th} + j\Psi)\tilde{E} + U(t) \qquad (2)$$

where A and Ψ are coefficients of the gain and phase change induced by the stimulated emission. G_{th} is the threshold gain level. The term $U(t)$ is a complex function describing the rate of change of $\tilde{E}(t)$ due to inclusion of the spontaneous emission in the stimulated emission. Mathematically, Ψ and A represent the real and the imaginary parts of the laser susceptibility, and vary with the injected carrier number N as follows [10], [25]:

$$A = \frac{a\xi}{V}(N - N_g) \qquad (3)$$

$$\Psi = \frac{\alpha a\xi}{V}(N - \overline{N}) \qquad (4)$$

where N_g is the carrier number at transparency, while $\overline{N}$ is the time-averaged carrier number. The parameter α is the so called "linewidth enhancement factor," and is given by [8], [10]

$$\alpha = \frac{\partial\Psi/\partial N}{\partial A/\partial N}. \qquad (5)$$

By writing the complex field amplitude in terms of the optical phase $\theta(t)$

$$\tilde{E}(t) = \left|\tilde{E}(t)\right| e^{j\theta(t)} \qquad (6)$$

we obtain the rate equations for the absolute value of the amplitude and phase as

$$\frac{d\left|\tilde{E}\right|}{dt} = \frac{1}{2}(A - G_{th})\left|\tilde{E}\right| + \text{Re}\left\{U(t)e^{-j\theta(t)}\right\} \qquad (7)$$

$$\frac{d\theta}{dt} = \frac{\alpha a\xi}{2V}(N - \overline{N}) + \frac{1}{\left|\tilde{E}\right|}\text{Im}\left\{U(t)e^{-j\theta(t)}\right\}. \qquad (8)$$

The fluctuation of the lasing frequency $\Delta\nu(t)$ is described by the variation of the optical phase as

$$\Delta\nu(t) = \frac{1}{2\pi}\frac{d\theta}{dt}. \qquad (9)$$

Equations (8) and (9) show how both the carrier number fluctuations and the random process of spontaneous emission induce the frequency fluctuations. The former effect induces variations in the refractive index of the active region which, in turn, changes the oscillating frequency ν.

Equations (7) and (8) can be given in terms of the photon number $S(t)$ by using the relation [26]

$$\frac{2\varepsilon}{\hbar\omega}\left|\tilde{E}\right|^2 = \begin{cases} S + 1, & \text{for optical emission} \\ S, & \text{for optical absorption} \end{cases} \qquad (10)$$

where ε is the dielectric constant of the active region. In expression (3) for the gain coefficient, the first term $a\xi N/V$ indicates optical emission, while the second term $a\xi N_g/V$ corresponds to optical absorption. Thus, (7) and (8) become

$$\frac{dS}{dt} = (A - G_{th})S + \frac{a\xi N}{V} + F_S(t) \qquad (11)$$

$$\frac{d\theta}{dt} = \frac{\alpha a\xi}{2V}(N - \overline{N}) + F_\theta(t) \qquad (12)$$

where

$$F_S(t) = \frac{4\varepsilon}{\hbar\omega}\left|\tilde{E}\right|\text{Re}\left\{U(t)e^{-j\theta(t)}\right\} \qquad (13)$$

and

$$F_\theta(t) = \frac{1}{\left|\tilde{E}\right|}\text{Im}\left\{U(t)e^{-j\theta(t)}\right\}. \qquad (14)$$

The functions $F_S(t)$ and $F_\theta(t)$ are Langevin noise sources. The mean values of these sources are zero, because the mean value of $U(t)$ is zero as follows:

$$\langle F_S(t)\rangle = \langle F_\theta(t)\rangle = 0. \qquad (15)$$

The autocorrelation functions of the noise sources are

$$\langle F_S(t)F_S(t')\rangle$$
$$= \left(\frac{4\varepsilon}{\hbar\omega}\right)^2\left|\tilde{E}\right|^2\left\langle\text{Re}\left\{U(t)e^{-j\theta(t)}\right\}\text{Re}\left\{U(t')e^{-j\theta(t')}\right\}\right\rangle$$
$$= V_{SS}\delta(t - t') \qquad (16)$$

$$\langle F_\theta(t)F_\theta(t')\rangle$$
$$= \frac{1}{\left|\tilde{E}\right|^2}\left\langle\text{Im}\left\{U(t)e^{-j\theta(t)}\right\}\text{Im}\left\{U(t')e^{-j\theta(t')}\right\}\right\rangle$$
$$= V_{\theta\theta}\delta(t - t') \qquad (17)$$

where V_{SS} and $V_{\theta\theta}$ are the variances of autocorrelations, and δ is Dirac's delta function.

Since $U(t)$ is a random complex function, we can assume

$$\left\langle\text{Re}\left\{U(t)e^{-j\theta(t)}\right\}\text{Re}\left\{U(t')e^{-j\theta(t')}\right\}\right\rangle$$
$$= \left\langle\text{Im}\left\{U(t)e^{-j\theta(t)}\right\}\text{Im}\left\{U(t')e^{-j\theta(t')}\right\}\right\rangle. \qquad (18)$$

Using this relation with (10), (16), and (17), we find that

$$V_{\theta\theta} = \frac{V_{SS}}{4(S+1)^2}. \tag{19}$$

The cross-correlation between $F_S(t)$ and $F_\theta(t)$ should be zero, because $\text{Re}\{U(t)e^{-j\theta(t)}\}$ and $\text{Im}\{U(t)e^{-j\theta(t)}\}$ are orthogonal, i.e.,

$$\langle F_S(t)F_\theta(t')\rangle = 0. \tag{20}$$

On the other hand, the rate equation of the carrier number N is

$$\frac{dN}{dt} = -AS - \frac{N}{\tau_s} + \frac{I}{e} + F_N(t) \tag{21}$$

where

τ_s carrier lifetime;
I injection current;
e electron charge.

The function $F_N(t)$ is the Langevin noise source on the carrier number, and is characterized mathematically by

$$\langle F_N(t)\rangle = 0 \tag{22}$$
$$\langle F_N(t)F_N(t')\rangle = V_{NN}\delta(t-t'). \tag{23}$$

The source $F_N(t)$ is cross-correlated with the photon number noise source $F_S(t)$, as well as with the phase noise source $F_\theta(t)$, which was not considered by previous calculations except the work of Abdulla and Saleh [14]

$$\langle F_S(t)F_N(t')\rangle = V_{SN}\delta(t-t') \tag{24}$$
$$\langle F_N(t)F_\theta(t')\rangle = V_{N\theta}\delta(t-t'). \tag{25}$$

The relation between V_{SN} and $V_{N\theta}$ is estimated by (13), (14), and (18) with (10) to be

$$V_{N\theta} = \frac{V_{SN}}{2(S+1)}. \tag{26}$$

Generating fluctuations on a quantum number forms a Poisson probability distribution, where the variance is equal to the mean value. Therefore, the variances V_{SS}, V_{NN} and V_{SN} are obtained from the rate equations (2), (11), and (21) as [3]–[5], [9]

$$V_{SS} = \left[\frac{a\xi}{V}(N+N_g)+G_{th}\right]S + \frac{a\xi N}{V} \tag{27}$$

$$V_{NN} = \frac{a\xi}{V}(N+N_g)S + \frac{N}{\tau_s} + \frac{I}{e} \tag{28}$$

$$V_{SN} = -\frac{a\xi}{V}[(N+N_g)S+N]. \tag{29}$$

The other variances of the generating fluctuation function $F_\theta(t)$ and $F_N(t)$ are determined via (19) and (26).

The output power $P(t)$ from the front facet of semiconductor lasers is given by

$$P(t) = \frac{h\nu c}{2n_r L} \frac{\ln(1/(R_f R_b))(1-R_f)}{(1-\sqrt{R_f R_b})(1+\sqrt{R_f/R_b})}S(t) \tag{30}$$

where

c speed of light in vacuum;
n_r, L refractive index and the length of the active region, respectively;
$h\nu$ photon energy of the emitted light;
R_f, R_b power reflectivities of the front and back facets, respectively.

B. Constructing Langevin Noise Sources

Obtaining explicit forms for the functions $F_S(t)$, $F_\theta(t)$, and $F_N(t)$ is necessary to perform numerical integration of (11), (12) and (21). Unless these noise sources are cross-correlated, we could numerically simulate them with three independent random generations using their auto-variances in (19), (27), and (28). Here, we demonstrate a general technique to simultaneously generate the cross-correlated noise sources $F_S(t)$, $F_N(t)$, and $F_\theta(t)$.

Equations (11), (12), and (21) are transformed into a new set of three equations of the photon number S, phase θ, and a variable defined as $kS + m\theta + N$ (where k and m are two real numbers)

$$\frac{dS}{dt} = (A - G_{th})S + \frac{a\xi N}{V} + F_S(t) \tag{11'}$$

$$\frac{d\theta}{dt} = \frac{\alpha a\xi}{2V}(N - \overline{N}) + F_\theta(t) \tag{12'}$$

$$\frac{d\{kS+m\theta+N\}}{dt} = k\left[(A-G_{th})S + \frac{a\xi N}{V}\right]$$
$$+ m\left[\frac{\alpha a\xi}{2V}(N-\overline{N})\right]$$
$$+ \left[-AS - \frac{N}{\tau_s} + \frac{I}{e}\right]$$
$$+ \{kF_S(t) + mF_\theta(t) + F_N(t)\}. \tag{31}$$

When the parameters k and m are defined as

$$k = -\frac{V_{SN}}{V_{SS}} \tag{32}$$

$$m = -\frac{V_{N\theta}}{V_{\theta\theta}} = 2k(S+1) \tag{33}$$

the noise functions $F_S(t)$, $F_\theta(t)$, and $kF_S(t)+mF_\theta(t)+F_N(t)$ become mutually orthogonal without cross-correlations among them so that we can define them independently. The auto-correlation of the new random function is

$$\langle\{kF_S(t)+mF_\theta(t)+F_N(t)\}$$
$$\cdot\{kF_S(t')+mF_\theta(t')+F_N(t')\}\rangle$$
$$= \{kV_{SN}+mV_{N\theta}+V_{NN}\}\delta(t-t')$$
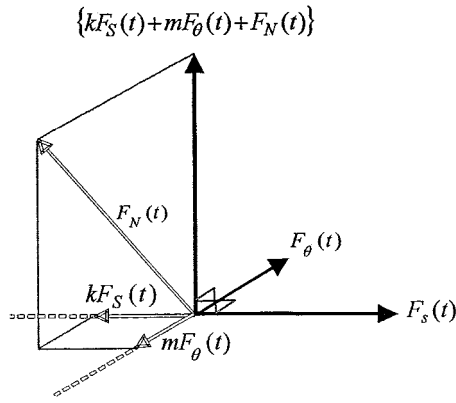$$= \{V_{NN}+2kV_{SN}\}\delta(t-t'). \tag{34}$$

Fig. 1. Schematic representation of the mutual correlations among the functions $F_S(t)$, $F_\theta(t)$, $F_N(t)$, and $kF_S(t) + mF_\theta(t) + F_N(t)$. A vector represents each function. The vector $kF_S(t) + mF_\theta(t) + F_N(t)$ is orthogonal to both $F_S(t)$ and $F_\theta(t)$ using appropriate settings of k and m.

TABLE I
VALUES OF THE PARAMETERS USED IN THE PRESENT COMPUTER SIMULATION OF A BURIED HETEROSTRUCTURE AlGaAs LASER

Symbol	Parameter	Value	Unit
a	Slope coefficient of the gain	2.75×10^{-12}	m^3s^{-1}
ξ	Optical field confinement factor	0.2	--
N_g	Carrier number at transparency	1.89×10^8	--
G_{th}	Threshold gain level	5.01×10^{11}	s^{-1}
α	Linewidth enhancement factor	2	--
τ_s	Electron lifetime	2.79×10^{-9}	s
n_r	Refractive index of the active region	3.59	--
V	Active region volume	75	μm^{-3}
L	Active region length	300	μm
R_f	Power reflectivity of the front facet	0.2	--
R_b	Power reflectivity of the back facet	0.7	--

In analogy with the vector notation, the orthogonal functions $F_S(t)$, $F_\theta(t)$ and $kF_S(t) + mF_\theta(t) + F_N(t)$ can form a 3-D functional space in which the function $F_N(t)$ can be represented as the linear combination

$$F_N(t) = \{kF_S(t) + mF_\theta(t) + F_N(t)\} - kF_S(t) - mF_\theta(t) \tag{35}$$

which satisfies relations (23)–(25). The idea of orthogonalization of the functions is illustrated in Fig. 1.

The delta functions appearing in the auto- and cross-correlation functions are treated in the numerical calculation such that

$$\langle F_a(t)F_b(t_i)\rangle = \begin{cases} \dfrac{1}{\Delta t} V_{ab}(t_i), & \text{for } |t - t_i| < \Delta t \\ 0, & \text{for } |t - t_i| > \Delta t \end{cases} \tag{36}$$

where $\Delta t = t_{i+1} - t_i$ is the time interval between sampling times of t_{i-1} and t_i. Since S, N, and θ vary with time, the variances V_{ab} (with a and b standing for any of S, N or θ) in (19), and (26)–(29) also vary with time. These variances at sampling time t_i are evaluated from the corresponding values
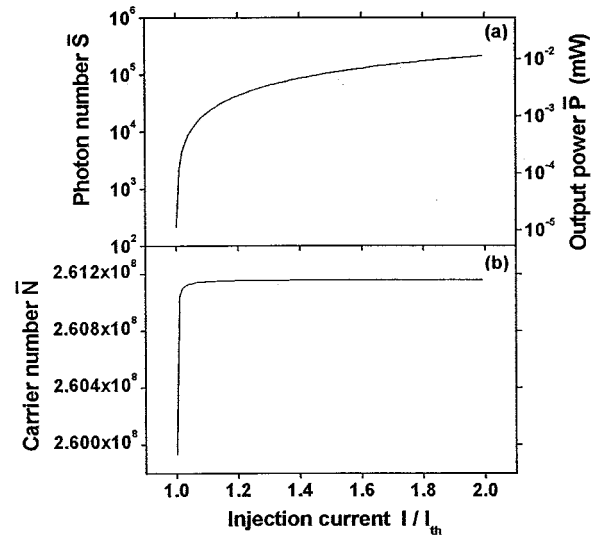

Fig. 2. Dependence of the dc values of: (a) the photon number $\overline{S}$, and (b) the carrier number $\overline{N}$ on the injection current I. Corresponding L–I characteristics are also given in (a) with the right-hand vertical axis.

at the preceding time t_{i-1} by supposing a quasisteady state ($dS/dt \approx dN/dt \approx 0$) during the time interval Δt, as in the following equations:

$$V_{SS}(t_i) = 2\frac{a\xi}{V} N(t_{i-1})[S(t_{i-1}) + 1] \tag{37}$$

$$V_{NN}(t_i) = 2\left[1 + \frac{a\xi\tau_s}{V} S(t_{i-1})\right] \frac{N(t_{i-1})}{\tau_s} \tag{38}$$

$$V_{SN}(t_i) = -\frac{a\xi}{V} [(N(t_{i-1}) + N_g)S(t_{i-1}) + N(t_{i-1})] \tag{39}$$

$$V_{\theta\theta}(t_i) = \frac{V_{SS}(t_i)}{4(S(t_{i-1}) + 1)^2} \tag{40}$$

$$V_{N\theta}(t_i) = \frac{V_{SN}(t_i)}{2(S(t_{i-1}) + 1)}. \tag{41}$$

By supposing g_S, g_θ, and g_N to be independent random numbers forming Gaussian probability distribution functions with zero mean values of $\langle g_S\rangle = \langle g_\theta\rangle = \langle g_N\rangle = 0$, and unity variances $\langle g_S^2\rangle = \langle g_\theta^2\rangle = \langle g_N^2\rangle = 1$ for ensembles of time, the noise sources $F_S(t_i)$, $F_\theta(t_i)$, and $kF_S(t_i) + mF_\theta(t_i) + F_N(t_i)$ are expressed as

$$F_S(t_i) = \sqrt{\frac{V_{SS}(t_i)}{\Delta t}} g_S \tag{42}$$

$$F_\theta(t_i) = \frac{1}{2[S(t_{i-1}) + 1]} \sqrt{\frac{V_{SS}(t_i)}{\Delta t}} g_\theta \tag{43}$$

$$\begin{aligned} k(t_i)F_S(t_i) &+ m(t_i)F_\theta(t_i) + F_N(t_i) \\ &= \sqrt{\frac{V_{NN}(t_i) + 2k(t_i)V_{SN}(t_i)}{\Delta t}} g_N. \end{aligned} \tag{44}$$

Finally, we generate the noise source $F_N(t_i)$ by substituting (42)–(44) into (35).

Thus, we can integrate (11), (12), and (21) using the generated forms of $F_S(t_i)$, $F_\theta(t_i)$, and $F_N(t_i)$, or equivalently the system of equations (11′), (12′), and (31) with forms (42)–(44).
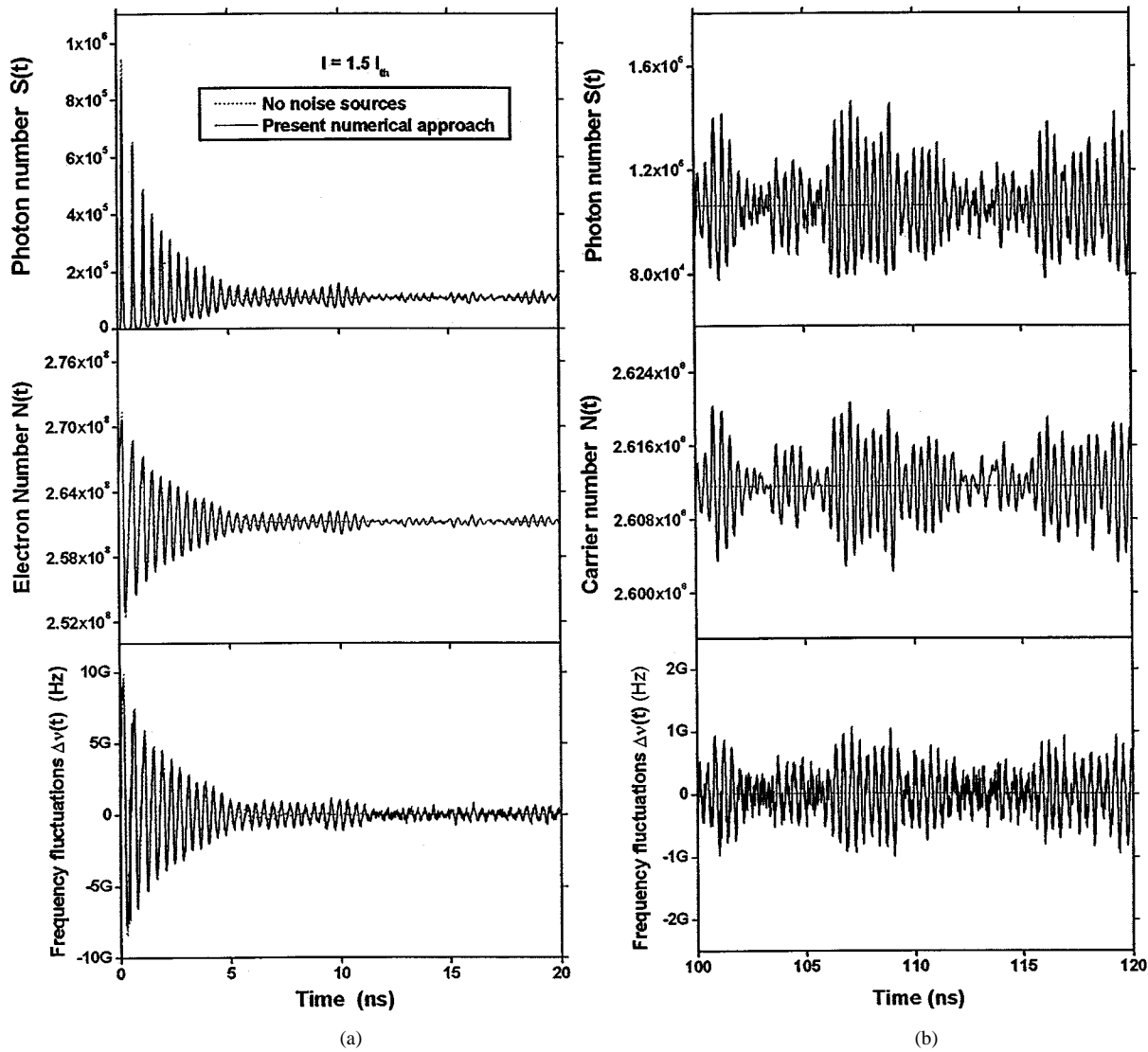
Fig. 3. Time-variations of the photon number $S(t)$, the carrier number $N(t)$, and the instantaneous frequency fluctuations $\Delta\nu(t)$: (a) during transients and (b) after termination of transients. Characteristics without the noise sources $F_S(t)$, $F_\theta(t)$, and $F_N(t)$ (dashed lines) are included for comparison. These quantities fluctuate around their dc values even after the termination of transients.

C. Noise and Spectral Linewidth

Most of the previous calculations of noise were based on small-signal analysis, which was developed by McCumber [3] and applied to semiconductor lasers by Haug [4]. In such an analysis, the time-fluctuating components are transformed into Fourier frequency components from which the noise and linewidth are calculated. The small-signal analysis of the proposed model is shown in the Appendix.

In the present numerical approach, the relative intensity noise (RIN) and the frequency, or phase, noise (FN) are evaluated from the fluctuations $\delta P(t)(=P(t)-\overline{P})$ and $\Delta\nu(t)$, respectively, that result from time integration of (11), (12), and (21) and using (9) and (30). The spectra of the RIN and FN are originally defined as the Fourier transform of the auto-correlation functions

$$\text{RIN} = \frac{1}{\overline{P}^2} \int_0^\infty \delta P(t)\delta P(t+\tau)e^{j\omega\tau}\, d\tau \qquad (45)$$

$$\text{FN} = \int_0^\infty \Delta\nu(t)\Delta\nu(t+\tau)e^{j\omega\tau}\, d\tau \qquad (46)$$

and are calculated over a long time period T from the equations

$$\begin{aligned}\text{RIN} &= \frac{1}{\overline{P}^2}\left\{\frac{1}{T}\int_0^T\left[\int_0^\infty \delta P(t)\delta P(t+\tau)e^{j\omega\tau}\, d\tau\right] dt\right\}\\ &= \frac{1}{\overline{P}^2}\left\{\frac{1}{T}\left|\int_0^T \delta P(\tau)e^{-j\omega\tau}\, d\tau\right|^2\right\} \qquad (47)\end{aligned}$$

$$\begin{aligned}\text{FN} &= \frac{1}{T}\int_0^T\left[\int_0^\infty \Delta\nu(t)\Delta\nu(t+\tau)e^{j\omega\tau}\, d\tau\right] dt\\ &= \frac{1}{T}\left|\int_0^T \Delta\nu(\tau)e^{-j\omega\tau}\, d\tau\right|^2 \qquad (48)\end{aligned}$$

where ω is the Fourier angular frequency.

The laser linewidth, the full-width at half-maximum (FWHM) of the single-mode spectrum, is determined from the low-frequency component of the FN as [12]

$$\Delta f = 4\pi\text{FN}|_{\omega=0}. \qquad (49)$$

III. NUMERICAL SIMULATION AND DISCUSSION

Numerical calculation of the photon number $S(t)$, carrier number $N(t)$, instantaneous frequency shift $\Delta\nu(t)$, and the corresponding noise terms are presented in this section. Typical values of AlGaAs laser parameters that appeared in the system of (11), (12), and (21) are listed in Table I. The corresponding (L–I) characteristics are plotted in Fig. 2(a) through the application of (30). The corresponding dc-values of the photon number $\overline{S}$ and the carrier number $\overline{N}$ are also plotted in Fig. 2(a) and (b), respectively. Applying the fourth-order Runge–Kutta method using a short time interval of $\Delta t = 10$ ps was the means for carrying out the numerical integrations. This small value of Δt results in noise sources that approximately describe a white noise spectrum up to a frequency of 100 GHz ($=1/\Delta t$), which is much higher than the relaxation frequency [15]. The integration has been extended to a time period as long as 40 μs, which requires more than 4 million integration steps.

Each of the independent Gaussian random variables g_S, g_θ and g_N are generated with the aid of the computer. The technique for generating the Gaussian random variables is as follows [27]. Two uniformly distributed random numbers u_1 and u_2 ranging between -1 and 1 are obtained from the computer random number generator. Then, following the Box–Muller transformation [28], we calculate each of the Gaussian random variables as one of the deviates

$$g_a = \begin{cases} \sqrt{-2\log u_1}\cos(2\pi u_2) \\ \text{or} \\ \sqrt{-2\log u_1}\sin(2\pi u_2) \end{cases}, \qquad a = S,\, N,\, or\, \theta \quad (50)$$

in an alternative way. The generated Gaussian random variables vary between -5 and 5.

### A. Fluctuations of the Photon and Carrier Numbers and the Oscillating Frequency

The time-varying profiles of the photon number $S(t)$, the carrier number $N(t)$, and the frequency fluctuations $\Delta\nu(t)$, calculated at an injection current I of 1.5 times the threshold value I_{th}, are plotted in Fig. 3(a) and (b) during and after the termination of transients, respectively. For comparison, the corresponding time variations when ignoring the fluctuation functions $F_S(t)$, $F_\theta(t)$, and $F_N(t)$ in (11), (12), and (21) are included in the figures. As shown in the figures, the effect of driving the rate equations by the Langevin noise sources is to fluctuate these physical quantities around their dc values. The fluctuations continue with time, even after the transient phenomena die away. The root-mean-square of the fluctuations over the integration time length T is about 14.5% of $\overline{P}$, which is comparable to the range observed by Gonda and Mukai [29].

B. Intensity Noise, Frequency Noise, and Linewidth

The quantum RIN and FN are calculated via (47) and (48), respectively, using the FFT. The effect of transients on calculations is avoided by counting the fluctuations after $t = 35$ ns. The simulated spectra of the RIN and FN are shown in Fig. 4(a)
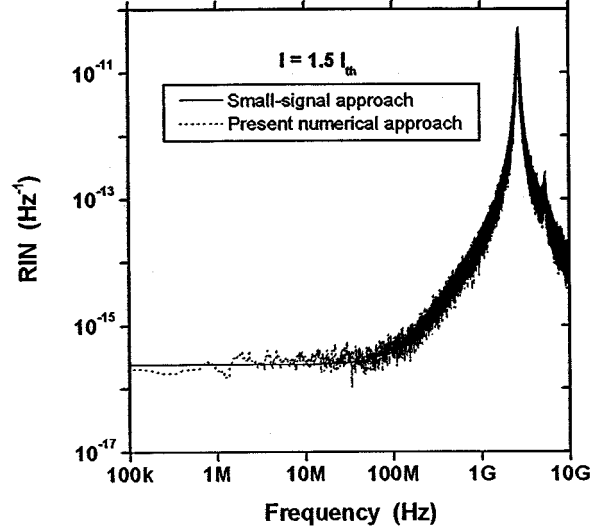
(a)
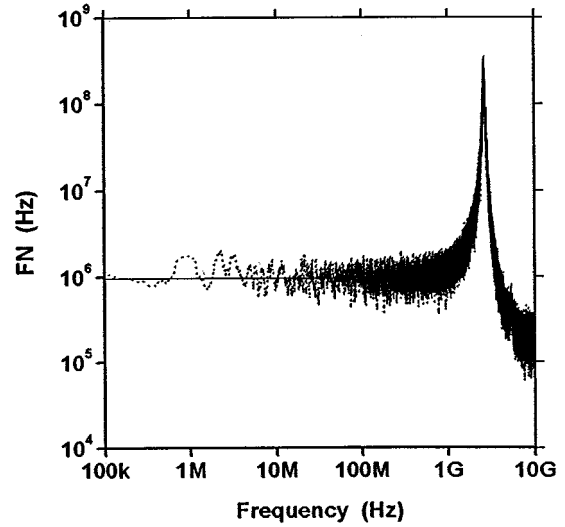
(b)

Fig. 4. Frequency spectra of: (a) quantum RIN and (b) quantum FN at injection current $I = 1.5I_{th}$. The spectra peak around the resonance frequency f_r and are almost flat in the low-frequency regime. The characteristics are a good fit with those calculated by the small-signal analysis.

and (b). Around the relaxation frequency f_r, both the RIN and FN show the pronounced peak that was detected in experiments [30]–[32]. At low frequencies, the FN is flatter than RIN. These characteristics are in good agreement with those determined by the small-signal approximation described by (A5) and (A6) in the Appendix.

As given in (49), the laser linewidth Δf is determined by extending the calculation of FN to very low frequencies ($\omega \approx 0$). Although this is very difficult when using the short integration step $\Delta t = 10$ ps from the computational point of view, the flatness of the FN at the low-frequency side enabled us to approximately calculate Δf at frequencies as low as 100 kHz. The calculated value at the injection level $I = 1.5I_{th}$ is $\Delta f = 11$ MHz which is comparable to the value 11.9 MHz obtained from (A11) in the Appendix, based on the small-signal approximation.
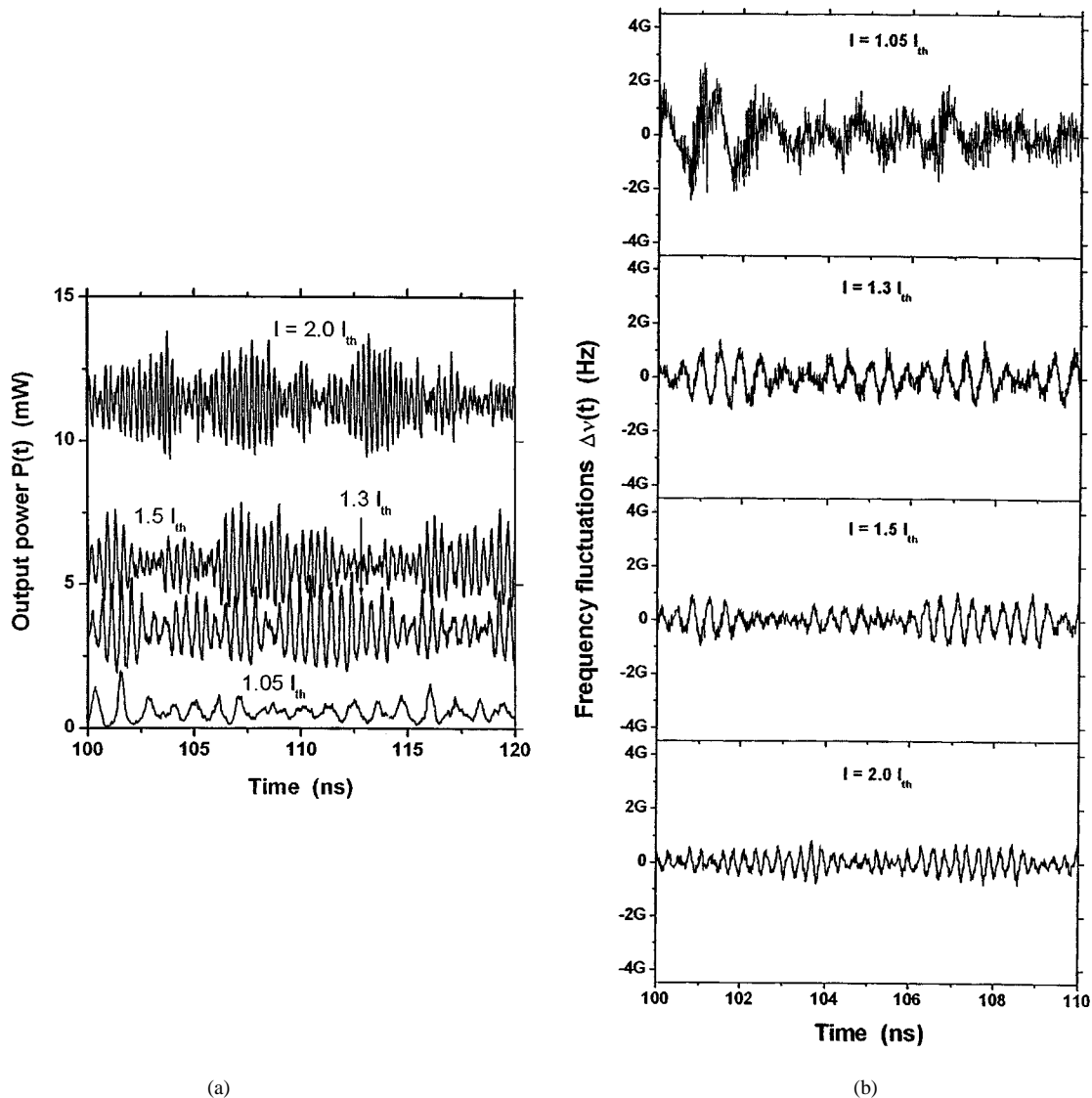
(a)   (b)

Fig. 5.   Instantaneous fluctuations of: (a) the output power $P(t)$ and (b) the oscillating frequency shift $\Delta \nu(t)$ far from the relaxation regime at different injection currents. The fluctuations are suppressed while their repetition becomes faster when I increases.

C. Dependence on Injection Current

The output power $P(t)$ and the frequency shift $\Delta \nu(t)$ at different injection currents I are shown in Fig. 5(a) and (b). The plotted fluctuations are far from the relaxation regime. A common feature of both variations is that the repetition of the fluctuations becomes faster with increasing I, which indicates an increase of the relaxation frequency f_r. The dependence of the fluctuations on I is further illuminated by collecting statistics for both $P(t)$ and $\Delta \nu(t)$. Fig. 6(a) and (b) plot the probability distributions of $P(t)$, normalized to the corresponding dc-power $\overline{P}$, and $\Delta \nu(t)$, respectively, at different injection levels. In these calculations, both $P(t)$ and $\Delta \nu(t)$ are counted over a long time interval (1 μs). The probability of $P(t)$ is calculated for powers in the range $P(t): 0 \rightarrow 2\overline{P}$, while that of $\Delta \nu(t)$ is done over the interval of $\Delta \nu(t): -1$ GHz $\rightarrow$ 1 GHz.

Although Fig. 5(a) indicates an increase in the amplitude of the power fluctuations with increasing I, the fluctuations are

actually suppressed as proved by the higher and narrower probability distributions at higher currents as shown in Fig. 6(a). The standard deviation of the fluctuations was found to decrease from $0.68\overline{P}$ near threshold $I = 1.05I_{th}$ to $0.067\overline{P}$ far from threshold $I = 2.0I_{th}$. Similarly, the fluctuations of the oscillating frequency $\Delta \nu(t)$ are suppressed and become regular with increasing current I, as shown in Fig. 5(b). This result is also confirmed by the results of the corresponding probability distributions given in Fig. 6(b). The distribution becomes narrower and higher with increasing I. Suppression of both power and frequency fluctuations occurs because when the current is far from threshold, the contribution of the random spontaneous transitions to the emitted light can be neglected when compared to the stimulated transitions and, hence, the emitted light becomes more coherent.

The corresponding spectra of the RIN and FN are plotted in Fig. 7(a) and (b), respectively. The variations of noise characteristics shown are in correspondence with those of the fluctuations
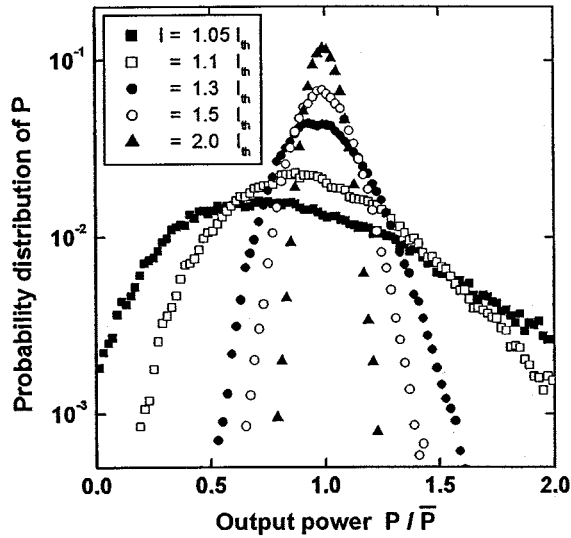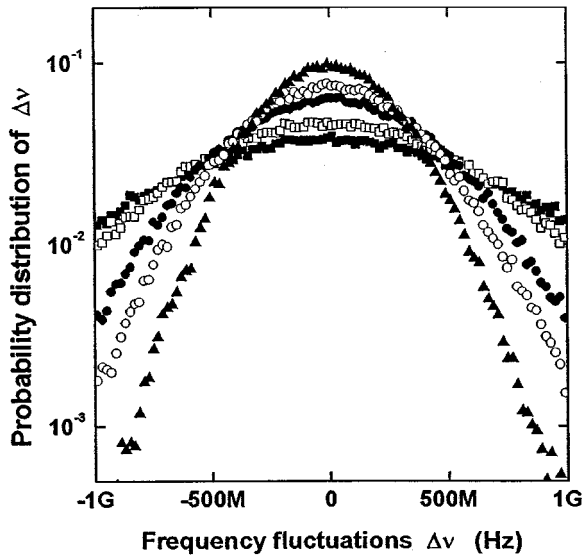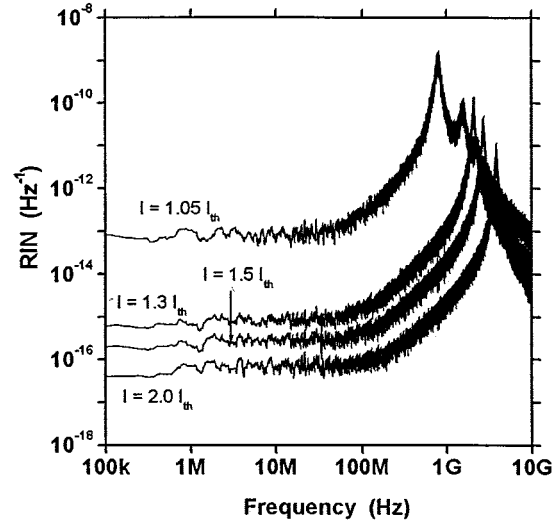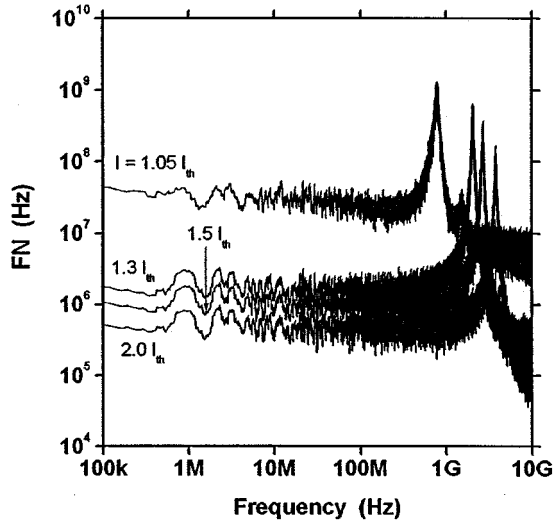
Fig. 6. The probability distributions of: (a) the output power $P(t)$ and (b) the frequency fluctuations $\Delta\nu(t)$ at different injection levels. High and narrow distributions are shown at high current values.

Fig. 7. Variation of the spectra of: (a) the intensity noise RIN and (b) the frequency noise FN with current I. Increasing I causes shift of the peak frequency and decrease of the noise level.

of $P(t)$ and $\Delta\nu(t)$ in Fig. 5. That is, the increase of the repetition of the fluctuations with increasing I corresponds to a shift of the peak frequency of both the RIN and FN spectra toward the higher frequency side. On the other hand, the suppression of the fluctuations leads to a decrease in the level of both RIN and FN with I, as shown in Fig. 7.

Fig. 8 plots the corresponding results of the linewidth Δf. The figure proves the rapid narrowing of Δf with increasing I near threshold [12]. The decrease of Δf with I matches the corresponding decrease of the FN shown in Fig. 6(b). Fig. 8 also plots the corresponding variation of the contributions to the frequency noise and linewidth: namely the carrier number fluctuations, spontaneous emission, and the correlation of the Langevin noise sources $F_N(t)$ and $F_\theta(t)$. The noise due to the

carrier number shows the highest contribution, while the noise due to the cross-correlation of $F_N(t)$ and $F_\theta(t)$ is several orders of magnitude lower, and can be neglected in the present model of intrinsic phase fluctuations. Nevertheless, the latter source might be enhanced or suppressed, especially near threshold, when operating with multi-modes or under optical feedback. The dependence of the linewidth Δf on the injection current is then typically described by the modified Schawlow–Townes relation [12]

$$\Delta f = \frac{eG_{th}^2(1+\alpha^2)}{2\pi(I - I_g/I_{th})(I - I_{th})} \tag{51}$$
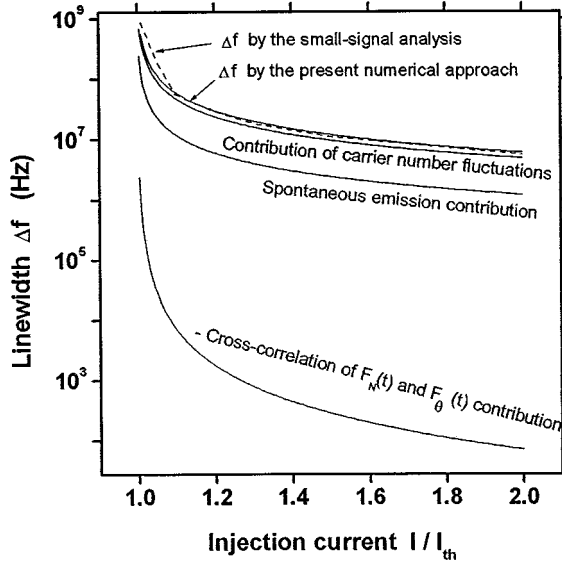
where $I_g = eVN_g/\tau_s$ is the current at transparency.

Fig. 8. Variation of the linewidth Δf with current I at a frequency as low as 100 kHz. The corresponding variations of the mechanisms contributing to broadening of Δf are also shown. The figure shows the rapid narrowing of Δf with increasing I near threshold.

D. Effect of Ignoring the Carrier Number Noise Source

Henry assumed that the carrier number noise source $F_N(t)$ has a negligible contribution to the phase fluctuations [7], [8]. Other authors followed the assumption by Henry, even when calculating the intensity noise [17], [20], [23]. In this subsection, we examine this assumption by comparing our results with other results with the assumption that $F_N(t) = 0$.

Fig. 9(a) plots the calculated RIN data for both the cases of $F_N(t) = 0$ and $F_N(t) \neq 0$ at $I = 2.0I_{th}$. As found in the figure, the characteristics in the high-frequency regime (including the peak position) are unaffected, while the RIN values are overestimated at low frequencies when the source $F_N(t)$ is ignored. The reason behind this effect can be traced to the small-signal analysis discussed in the Appendix. The RIN at low frequencies in this case is given by

$$\text{RIN}|_{F_N(t)=0} = \frac{1}{\overline{S}^2|Y|^2} \left(\frac{a\xi}{V} \overline{S} + \frac{1}{\tau_s} \right)^2 \langle F_{S\omega}^2 \rangle \tag{52}$$

which does not depend on the cross-correlation $\langle F_{S\omega} F_{N\omega} \rangle$. Since $\langle F_{S\omega} F_{N\omega} \rangle$ has negative values and then contributes to reduce the RIN as given in (24) and (29), the assumption of $F_N(t) = 0$ brings the RIN to a larger value. The dependence of such a discrepancy in the RIN on the current I in the low-frequency regime is illustrated in Fig. 9(b). The overestimation of RIN is larger at higher injection levels. Then, inclusion of the noise source $F_N(t)$ in the rate equations is necessary for accurate analysis of the noise.

Regarding the frequency noise, we did not find a big difference between the calculated data. The fluctuation source $F_N(t)$ may affect the intensity fluctuations more than the frequency fluctuations.
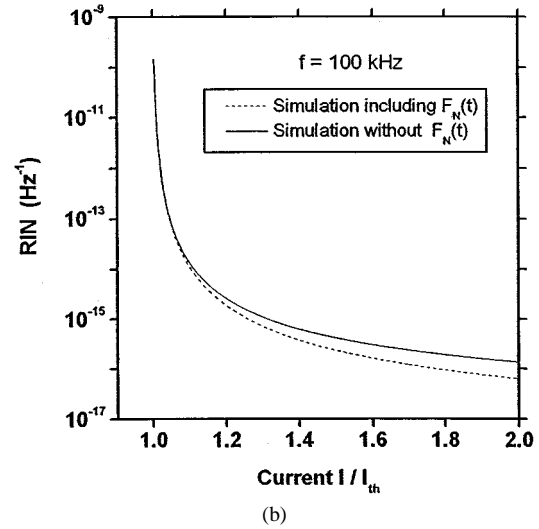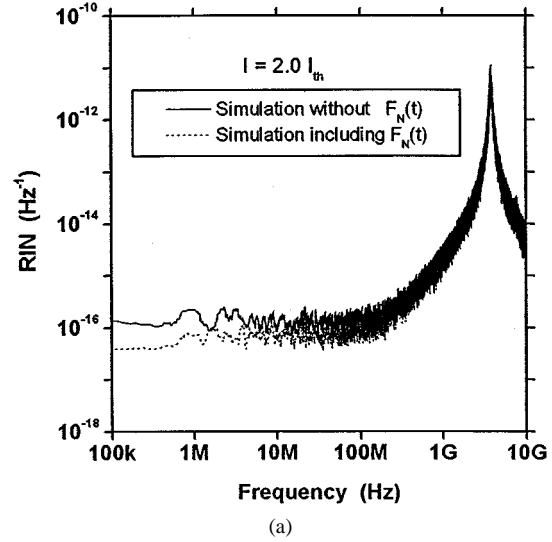

(a)

(b)

Fig. 9. Effect of ignoring the carrier noise source $F_N(t)$ on the: (a) spectrum of RIN at $I = 2.0I_{th}$ and (b) RIN values at the low frequency of 100 kHz. RIN is overestimated when $F_N(t) = 0$ in the low-frequency regime at injection levels far from threshold.

IV. CONCLUSION

Numerical simulations of intensity and phase noise in semiconductor lasers are demonstrated. A new technique is devised to generate the correlated Langevin noise sources on the photon and carrier numbers, as well as on the phase of the lasing field. Simulations of line-shape broadening and its dependence on the injection current are analyzed. The results are in agreement with those obtained by small-signal analysis. Contributions of the carrier-number noise source and its cross-correlation with the phase noise source to intensity and phase noise are examined for the first time. Our proposed model will be applied to analyze complicated phenomena under optical feedback with suitable extensions of the model.

APPENDIX

Here, we show the application of the small-signal analysis to calculate the spectral dependence of both the RIN and FN.

The frequency components of the fluctuation functions $F_S(t)$, $F_\theta(t)$, and $F_N(t)$ are defined through the Fourier transform

$$F_a(t) = \int_{-\infty}^{\infty} F_{a\omega} e^{j\omega t} \, d\omega \tag{A1}$$

where the symbol a stands for each of S, θ, and N. Both the photon number $S(t)$ and the carrier number $N(t)$ are assumed to have fluctuations as

$$S(t) = \overline{S} + \delta S(t) = \overline{S} + \int_{-\infty}^{\infty} S_\omega e^{j\omega t} \, d\omega \tag{A2a}$$

$$N(t) = \overline{N} + \delta N(t) = \overline{N} + \int_{-\infty}^{\infty} N_\omega e^{j\omega t} \, d\omega \tag{A2b}$$

and the frequency fluctuations are transformed as

$$\Delta\nu(t) = \int_{-\infty}^{\infty} \Delta\nu_\omega e^{j\omega t} \, d\omega \tag{A2c}$$

with S_ω, N_ω and $\Delta\nu_\omega$ being the corresponding fluctuating components in the frequency domain.

By substituting the above equations in (11), (12) and (21), and assuming that the fluctuations S_ω and N_ω are so small that $\overline{S} \gg S_\omega$ and $\overline{N} \gg N_\omega$, the equations are linearized for both the dc components and the fluctuating components so as to the following two system of equations:

$$\left[\frac{a\xi}{V}(\overline{N} - N_g) - G_{th}\right]\overline{S} + \frac{a\xi}{V}\overline{N} = 0 \tag{A3a}$$

$$\frac{a\xi}{V}(\overline{N} - N_g)\overline{S} + \frac{\overline{N}}{\tau_s} = \frac{I}{e} \tag{A3b}$$

$$\left(j\omega + \frac{a\xi\overline{N}}{V\overline{S}}\right)S_\omega - \frac{a\xi}{V}(\overline{S}+1)N_\omega = F_{S\omega} \tag{A4a}$$

$$\frac{a\xi}{V}(\overline{N} - N_g)S_\omega + \left(j\omega + \frac{a\xi\overline{S}}{V} + \frac{1}{\tau_s}\right)N_\omega = F_{N\omega} \tag{A4b}$$

$$\Delta\nu_\omega = \frac{1}{2\pi}\left(\frac{a\xi\alpha}{2V}N_\omega + F_{\theta\omega}\right). \tag{A4c}$$

We calculate the dc-values $\overline{S}$ and $\overline{N}$ by solving (A3a) and (A3b), and then solve the system of equations (A4) for the fluctuation components S_ω and N_ω. Both RIN and FN are then determined with the ensemble averages of the square values of the fluctuations

$$\text{RIN} = \frac{\langle S_\omega^2 \rangle}{\overline{S}^2} \tag{A5}$$

$$\begin{aligned}\text{FN} &= \langle \Delta\nu_\omega^2 \rangle \\ &= \frac{1}{4\pi^2}\left\{\left(\frac{\alpha a\xi}{2V}\right)^2\langle N_\omega^2\rangle + \langle F_{\theta\omega}^2\rangle \frac{\alpha a\xi}{V}\,\text{Re}\langle N_\omega F_{\theta\omega}\rangle\right\}\end{aligned} \tag{A6}$$

where the noise on the photon number and the carrier number, as well as the noise due to correlation of the fluctuations on the carrier number and the phase are given, respectively, by

$$\begin{aligned}\langle S_\omega^2 \rangle = \frac{1}{|Y|^2}&\left\{\left[\omega^2 + \left(\frac{1}{\tau_s} + \frac{a\xi}{V}\overline{S}\right)^2\right]\langle F_{S\omega}^2\rangle\right. \\ &+ \left(\frac{a\xi}{V}(\overline{S}+1)\right)^2\langle F_{N\omega}^2\rangle \\ &\left.+ 2\frac{a\xi}{V}\left(\frac{1}{\tau_s} + \frac{a\xi}{V}\overline{S}\right)(\overline{S}+1)\langle F_{S\omega}F_{N\omega}\rangle\right\}\end{aligned} \tag{A7a}$$

$$\begin{aligned}\langle N_\omega^2 \rangle = \frac{1}{|Y|^2}&\left\{\left(\omega^2 + \left(\frac{a\xi}{V}\right)^2\frac{\overline{N}^2}{\overline{S}^2}\right)\langle F_{N\omega}^2\rangle\right. \\ &+ \left(\frac{a\xi}{V}\right)^2(\overline{N} - N_g)^2\langle F_{S\omega}^2\rangle \\ &\left.- 2\left(\frac{a\xi}{V}\right)^2\frac{\overline{N}}{\overline{S}}(\overline{N} - N_g)\langle F_{S\omega}F_{N\omega}\rangle\right\}\end{aligned} \tag{A7b}$$

$$\langle N_\omega F_{\theta\omega}\rangle = \frac{1}{Y}\left(j\omega + \frac{a\xi}{V}\frac{\overline{N}}{\overline{S}}\right)\frac{\langle F_{S\omega}F_{N\omega}\rangle}{2(\overline{S}+1)}. \tag{A7c}$$

The term Y in the denominator is given by

$$Y = \omega_r^2 - \omega^2 + j\omega\left[\frac{1}{\tau_s} + \frac{a\xi}{V}\overline{S} + \frac{a\xi}{V}\frac{\overline{N}}{\overline{S}}\right] \tag{A8}$$

where ω_r is the angular relaxation frequency, and is given by

$$\begin{aligned}\omega_r^2 &= (2\pi f_r)^2 \\ &= \frac{a\xi}{\tau_s V}\left\{\frac{\overline{N}}{\overline{S}}\left(1 + \frac{a\xi\tau_s}{V}\overline{S}\right) + \frac{a\xi\tau_s}{V}(\overline{S}+1)(\overline{N} - N_g)\right\}.\end{aligned} \tag{A9}$$

Therefore, the noise is determined by the correlations $\langle F_{a\omega}F_{b\omega}\rangle$, with a and b standing for either S, θ, or N, in the frequency domain. These correlations are the frequency components of the corresponding correlation functions $\langle F_a(t)F_b(t')\rangle$ in the time domain and are determined as the time averages of their variances

$$\langle F_{a\omega}F_{b\omega}\rangle = \overline{V_{ab}}. \tag{A10}$$

These time-averaged variances are calculated via (19) and (26)–(29) using the dc values $\overline{S}$ and $\overline{N}$.

Finally, the spectral full-linewidth is determined from the low-frequency component of the FN as [9]

$$\Delta f = 4\pi\langle \Delta\nu_0^2\rangle. \tag{A11}$$

REFERENCES

[1] A. L. Schawlow and C. H. Townes, "Infrared and optical masers," *Phys. Rev.*, vol. 112, pp. 1940–1949, 1958.

[2] G. P. Agrawal and N. K. Dutta, *Semiconductor Lasers*. New York: Van Nostrand Reinhold, 1993.

[3] D. E. McCumber, "Intensity fluctuations in the output of CW laser oscillators," *Phys. Rev.*, vol. 141, pp. 306–322, 1966.

[4] H. Haug, "Quantum-mechanical rate equations for semiconductor lasers," *Phys. Rev.*, vol. 184, pp. 338–348, 1969.

[5] T. Paoli, "Near-threshold behavior of the intrinsic resonant frequency in a semiconductor laser," *IEEE J. Quantum Electron.*, vol. QE-15, pp. 807–812, 1979.

[6] G. Arnold and K. Petermann, "Intrinsic noise of semiconductor lasers in optical communication systems," *Opt. Quantum Electron.*, vol. 12, pp. 207–219, 1980.

[7] C. H. Henry, "Theory of the phase noise and power spectrum of a single mode injection laser," *IEEE J. Quantum Electron.*, vol. QE-19, pp. 1391–1397, 1985.

[8] ——, "Phase noise in injection lasers," *IEEE J. Lightwave Technol.*, vol. LT-4, pp. 298–311, 1986.

[9] M. Yamada, "Theory of mode competition noise in semiconductor injection lasers," *IEEE J. Quantum Electron.*, vol. QE-22, pp. 1052–1059, 1986.

[10] ——, "Theoretical analysis of line-broadening due to mode-competition and optical feedback in semiconductor injection lasers," *Trans. IEICE*, vol. E71, pp. 152–160, 1988.

[11] G. P. Agrawal and G. R. Gray, "Intensity and phase noise in microcavity surface-emitting semiconductor lasers," *Appl. Phys. Lett.*, vol. 59, pp. 399–402, 1991.

[12] M. Yamada, "Variation of intensity noise and frequency noise with the spontaneous emission factor in semiconductor lasers," *IEEE J. Quantum Electron.*, vol. 30, pp. 1511–1519, 1994.

[13] D. Marcuse, "Computer simulation of laser photon fluctuations: Single-cavity laser results," *IEEE J. Quantum Electron.*, vol. QE-20, pp. 1148–1155, 1984.

[14] R. M. Abdula and B. E. A. Saleh, "Dynamic spectra of pulsed laser diodes and propagation in single-mode fibers," *IEEE J. Quantum Electron.*, vol. QE-22, pp. 2123–2130, 1986.

[15] N. Schunk and K. Petermann, "Noise analysis of injection-locked semiconductor injection lasers," *IEEE J. Quantum Electron.*, vol. QE-22, pp. 642–650, 1986.

[16] A. Mecozzi, S. Piazzolla, A. Sapia, and P. Spano, "Non-Gaussian statistics of frequency fluctuations in line-narrowed semiconductor lasers," *IEEE J. Quantum Electron.*, vol. QE-24, pp. 1985–1988, 1988.

[17] A. Czylwik, "A theoretical analysis of the transient intensity noise of semiconductor lasers," *IEEE J. Quantum Electron.*, vol. 25, pp. 39–46, 1989.

[18] J. C. Cartledge, "On the parabolistic characterization of side mode fluctuations in pulse-modulated nearly-single-mode semiconductor lasers," *IEEE J. Quantum Electron.*, vol. 26, pp. 2046–2051, 1990.

[19] J. Wang and K. Petermann, "Noise characteristics of PCM-modulated single-mode semiconductor laser diodes with distant optical feedback," *IEE Proc. J*, vol. 137, pp. 385–390, 1990.

[20] E. A. Avrutin, "Analysis of spontaneous emission and noise in self-pulsing laser diodes," *IEE Proc. J*, vol. 140, pp. 16–21, 1993.

[21] G. R. Gray, A. T. Ryan, G. P. Agrawal, and E. C. Gage, "Control of optical feedback induced laser intensity noise in optical data recording," *Opt. Eng.*, vol. 32, pp. 739–745, 1993.

[22] L. N. Langley and K. A. Shore, "Intensity noise and linewidth characteristics of laser diodes with phase conjugate optical feedback," *IEE Proc. Optoelectron.*, vol. 141, pp. 103–108, 1994.

[23] J. Y. Law and G. P. Agrawal, "Feedback-induced chaos and intensity-noise enhancement in vertical-cavity surface-emitting lasers," *J. Opt. Soc. Amer.*, vol. 15, pp. 562–569, 1998.

[24] D. Marcuse, "Computer simulation of laser photon fluctuations: Theory of single-cavity laser," *IEEE J. Quantum Electron.*, vol. QE-20, pp. 1139–1148, 1984.

[25] M. Ahmed and M. Yamada, "An infinite order perturbation approach to gain calculation in injection semiconductor lasers," *J. Appl. Phys.*, vol. 84, pp. 3004–3015, 1998.

[26] Y. Suematsu and A. R. Adams, *Hand Book of Semiconductor Lasers and Photonic Integrated Circuits*. London, U.K.: Chapman & Hall, 1994.

[27] W. H. Press, S. A. Teukolsky, W. T. Vetterling, and B. P. Flannery, *Numerical Recipes in Fortran: The Art of Scientific Computing*. Cambridge, MA: Cambridge Univ. Press, 1992.

[28] A. Stuart and J. K. Ord, *Advanced Theory of Statistics*. London, U.K.: Griffin, 1987.

[29] S. Gonda and S. Mukai, "Degradation and intensity fluctuations in CW AlGaAs double-heterostructure junction lasers," *IEEE J. Quantum Electron.*, vol. QE-11, pp. 545–550, 1975.

[30] L. A. D'Asaro, Sr., J. M. Cherlow, and T. L. Paoli, "Continuous microwave oscillations in GaAs junction lasers," *IEEE J. Quantum Electron.*, vol. QE-4, pp. 164–167, 1968.

[31] S. Piazolla, P. Spano, and M. Tamburrini, "Characterization of phase noise in semiconductor lasers," *Appl. Phys. Lett.*, vol. 41, pp. 695–696, 1982.

[32] Y. Yamamoto, "AM and FM quantum noise in semiconductor lasers—Part I: Theoretical analysis," *IEEE J. Quantum Electron.*, vol. QE-19, pp. 34–46, 1983.

Moustafa Ahmed (S'99–M'99) was born in Minia, Egypt, in 1966. He received the B.Sc. and M.Sc. degrees in physics from the Faculty of Science, Minia University, Minia, Egypt, in 1988 and 1993, respectively. In 1999, he received the Ph.D. Eng. degree from the Graduate School of Natural Science and Technology, Kanazawa University, Kanazawa, Japan. His Ph.D. work mainly involved developing design methods for optical filters, and an infinite-order approach to gain calculation in semiconductor lasers.

He is currently a Lecturer in the Physics Department, Minia University, Egypt. Since September 2000, he has been a Visiting Fellow at the Department of Electrical and Electronic Engineering, Kanazawa University, supported by the post-doctoral program of the Japan Society for the Promotion of Science (JSPS). His research interests are in the areas of opto-electronics and statics and dynamics of semiconductor lasers.

Minoru Yamada (M'82) was born in Yamanashi, Japan, in 1949. He received the B.S. degree in electrical engineering from Kanazawa University, Kanazawa, Japan, in 1971, and the M. S. and Ph.D. degrees in electronics engineering from the Tokyo Institute of Technology, Tokyo, Japan, in 1973 and 1976, respectively.

He joined Kanazawa University in 1976, where he is presently a Professor. His research is in semiconductor injection lasers, semiconductor modulators, and unidirectional optical amplifiers. From 1982 to 1983, he was a Visiting Scientist at Bell Laboratories, Holmdel, NJ.

Dr. Yamada received the Yonezawa Memorial Prize in 1975, the Paper Reward in 1976, and the Achievement Award in 1978 from the IECE of Japan.

Masayuki Saito was born in Hokkaido, Japan, in 1976. He received the B.S. degree in electrical and computer engineering from Kanazawa University, Kanazawa, Japan, in 1999, and the M.S. degree in electrical and electronic engineering from Tokyo Institute of Technology, Tokyo, Japan, in 2001.

In April 2001, he joined Kamakura Works, Mitsubishi Electric, Kamakura-shi, Japan. His research interest is in microwave engineering.